Application of First-Principles-Based Artificial Neural Network Potentials to Multiscale-Shock Dynamics Simulations on Solid Materials

Masaaki Misawa,[1] Shogo Fukushima,[2] Akihide Koura,[2] Kohei Shimamura,[2] Fuyuki Shimojo,[2] Subodh Tiwari,[3] Ken-ichi Nomura,[3] Rajiv K. Kalia,[3] Aiichiro Nakano,[3] and Priya Vashishta[3]*

[1]Graduate School of Natural Science and Technology, Okayama University, Okayama 700-8530, Japan

[2]Department of Physics, Kumamoto University, Kumamoto 860-8555, Japan

[3]Collaboratory for Advanced Computing and Simulations, University of Southern California, Los Angeles, CA 90089, USA

*E-mail: misawa@okayama-u.ac.jp

Artificial neural-network (ANN) potential trained with first-principles calculations have emerged as a promising approach for molecular dynamics (MD) simulations encompassing large space and time scales while retaining first-principles accuracy. However, the application of ANN-MD has thus far been limited to *near-equilibrium* processes. Here, we combine first principles-trained ANN-MD with multiscale shock theory (MSST) to successfully describe *far-from-equilibrium* shock phenomena. Our ANN-MSST-MD approach describes shock-wave propagation in solid with first-principles accuracy, but within 5,000-times shorter computing time. Accordingly, ANN-MD-MSST was able to resolve fine, long-time elastic deformation at low shock speed, which was impossible with first-principles MD due to the high computational cost. This work thus lays a foundation of ANN-MD simulation to study a wide range of far-from-equilibrium processes.

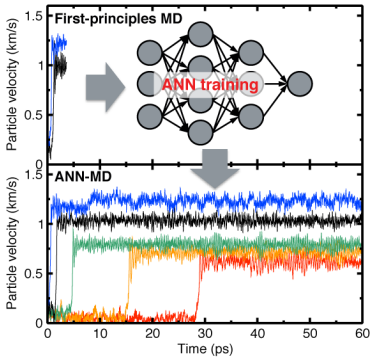

Investigating wave propagation properties and shock wave induced structural dynamics in Earth-abundant materials are important not only for geodynamics research but also to understand material processes[1-5]. For example, it is reported that silica (SiO_2) transforms into nano-polycrystalline form of stishovite, which is a high-pressure polymorph of silica, during high-pressure shock compression[1]. This nano-polycrystalline stishovite is nominated for next-generation high performance ceramics since its high hardness and toughness[6-9]. To study the atomistic scale dynamics in materials under such extreme conditions, molecular dynamics (MD) simulations exert great power because those are able to chase the atomic trajectories with extremely high time resolution of femto-second. Particularly, first-principles MD (FPMD) method based on the density functional theory (DFT) calculation provides us great insight into microscopic mechanisms of such complex phenomena at a viewpoint of electronic states. To treat wave propagation or shock-induced chemistry or structural transformation in materials, Reed *et al.*, proposed a multi-scale non-equilibrium MD technique using 1D Euler equation for compressible flow[10]. Using this multi-scale shock technique (MSST), atomistic behaviors at the shock wave front can be represented for long time scale. Combining MSST with FPMD method, it has succeeded to investigate mechanical response, chemical reaction, phase transition and its anisotropy of various materials under shock compression[11-13].

However, the computable space and time scales for FPMD simulations are limited on the order of several hundred atoms and tens picosecond (ps), because of its high computational costs. Therefore shock-induced structural transformations or chemical reactions that requires more than several tens ps (e.g. previously mentioned stishovite formation[1]) are difficult to investigate efficiently based on FPMD method. In order to solve this problem, many efforts have been made to extend computable space and time scales by reducing computational cost, while retaining first-principles accuracy[14-26]. In this trend, recently an empirical potential constructed based on artificial neural network (ANN) is attract a lot of attention as a solution of the computational cost issue[16-24]. The fundamental idea of this method is using the ANN that has learned the correlation of the atomic configuration and potential energy of the system, as an empirical potential energy

function. If the learning has achieved enough effectively, the computational cost of MD simulation with ANN-potential (ANN-MD) is reduced to classical MD (CMD) level while retaining FPMD accuracy at least for the reference configuration. To construct an empirical potential using ANN, the total energy of the system is defined as a sum of the atomic energy, and these atomic contributions are considered as output information of feed-forward neural networks (FFNNs). In addition of that, the Cartesian coordinates, which are obtained by first-principles calculations, are transformed into a set of basis functions that depict the local structural environment associated with each atom[17]. The basis function is defined as a set of atomic centered radial and angular functions that corresponds to bond length and bond angles around an atom, respectively[23-24]. The ANN-potentials constructed by this scheme are used for wide range of system, and provide excellent results[27-30]. However, there is no precedent for application to the shock propagation simulation so far.

In this work, we have attempted to perform shock simulation using the first-principles-based ANN-potential and to show that ANN-potentials have a potential application to the non-equilibrium MD simulation under extreme conditions. For the model system, α-quartz was employed and the elastic deformation reaction under shock compression has been calculated. The shock related quantities produced by the ANN-potential were compared with FPMD results, and the quality and potential application to the shock simulation of the ANN-potential was investigated. The main contribution of this paper is the first application of ANN to far-from-equilibrium processes, while retaining first-principles accuracy yet applicable to much larger spatiotemporal scales. This is achieved by combining ANN potential and MSST, with a specific illustrative application to shock-compressed quartz.

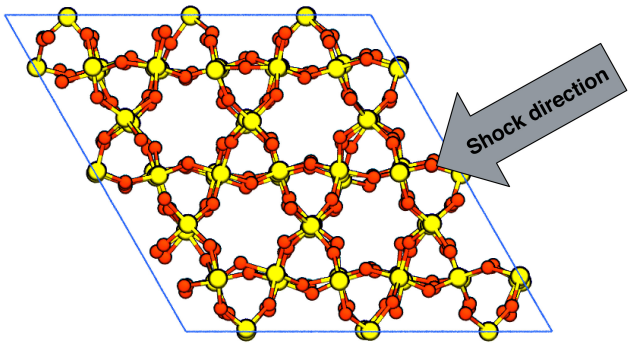

Figure 1. Schematic image of the shock-induced simulation. The yellow and red balls illustrate silicon and oxygen atoms, respectively. The blue line indicates periodic boundary of the simulation cell. Shock wave is induced along [2 1 0] direction, which is perpendicular to the (1 0 0) plane of α-quartz.

In order to obtain the first-principles-based atomistic behavior and prepare teaching data for learning of ANN-potential, shock simulations based on FPMD and MSST have been performed for α-quartz. First, we prepared a hexagonal simulation cell consisting 243 atoms ($Si_{81}O_{162}$), which corresponds to 3×3×3 of the crystal unit cell of α-quartz. During MD simulations, periodic boundary conditions for all directions are taken into account to the simulation cell. Next, to create initial configuration for the shock simulations, the crystal structure was relaxed by FPMD simulation with isothermal-isobaric (NPT) ensemble at an ambient conditions during 1500 step (1.82 ps). Then the shock simulations are carried out based on MSST for various shock speeds with a range of 6.0 to 7.4 km/s. The shock direction is set to [2 1 0] direction, which is perpendicular to (1 0 0) plane of α-quartz (Figure 1). For each shock conditions, FPMD simulations have been carried out until elastic or plastic deformation reactions were observed, at least 0.6 ps.

Using the ANN-potential that was constructed based on FPMD simulation data, ANN-MD shock simulations have been performed with the same simulation system as FPMD simulations. The time step, creating process of the initial configuration and shock direction was also the same as the FPMD. As the result of the shock simulation during 60.5 ps (= 50,000 steps) with the

ANN-potential, we observed elastic deformation behavior at the shock speed of from 5.7 to 6.4 km/s. In order to compare the calculation speed and quality of the ANN-potential, traditional CMD simulation with empirical interatomic pair potential also has been performed. The set up procedures and simulation conditions were same as the ANN-MD. Information of the empirical potential used in this work and results of CMD simulations with the empirical potential are summarized in the Supporting Information.

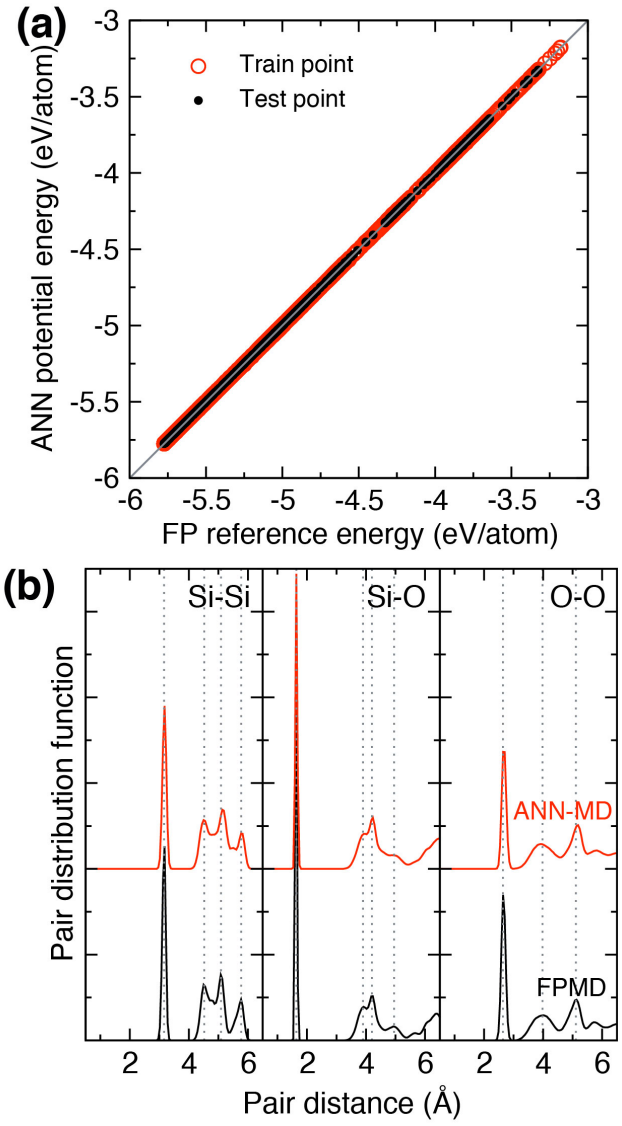

Figure 2. (a) Comparison of the potential energy predicted by the ANN-potential with corresponding potential energy in FPMD simulation. The red and black symbols indicate the potential energies for the training and test data set, respectively. The gray line is the ideal

diagonal line that shows to the location of zero-error points. (b) Pair distribution functions (PDFs) of un-shocked state at ambient conditions calculated from the FPMD (black) and ANN-MD (red). The left, middle and right sides display the PDF for Si-Si, Si-O and O-O pairs, respectively. The gray dotted lines indicate the position of major peaks in the FPMD result.

To confirm the quality of ANN-potential for energy and structures, first the total energies produced by the ANN-potential were compared with the corresponding reference energies obtained from FPMD (Figure 2a). We can see clearly that the ANN-potential provides accurate potential energy not only for atomic configuration of training data set but also that for testing data set. The final root mean squared errors (RMSE) of training and testing set were about 0.6 and 0.7 meV/atom, corresponding to a temperature of 6 and 7 K, respectively. According to that the temperature increased to more than 1,000 K and in some case exceeded 2,000 K when plastic deformation occurred in the FPMD simulations, this RMSE should be small enough.

Next, to confirm that the ANN potential provides accurate structural properties, the pair distribution functions (PDFs) of an un-shocked state were calculated using NPT ensemble under ambient conditions. In order to test the quality of ANN potential for structural properties more rigidly, additional FPMD simulation of 3,000 steps (~3.63 ps) was carried out, and PDF was calculated with these 3,000 configurations that does not used for the training of the ANN-potential. ANN-MD and CMD simulations were also carried out during 4500 steps, and PDFs were calculated using configurations of latest 3,000 steps. The calculated PDFs for FPMD and ANN-MD are compared in Figure 2b (CMD result is shown in Figure S1 in the Supporting Information). The major peak positions in the ANN-MD result show good agreement with that of the FPMD result, and the overall trends also consistent with each other. Even though the reference FPMD data calculated with un-shocked ambient conditions was less than 6% of all reference data, the ANN-potential provided structural properties very well. In the MD simulations for un-shocked ambient conditions, the computational speed was also compared with each other. When using the same number of cores (in this study, 96 cores) for the computation, the computational time of ANN-MD was more than 5,000 times shorter than that of FPMD, and

about 7 times longer than that of CMD. This result suggests that the ANN-MD may bear long-term simulation such as sub-microseconds for several hundred particles system. To summarize the analysis thus far, it can be expected that the ANN-potential created in this work reproduce energetic and structural properties with high accuracy at least for the reference structures, with dramatic reduction of the computational costs.

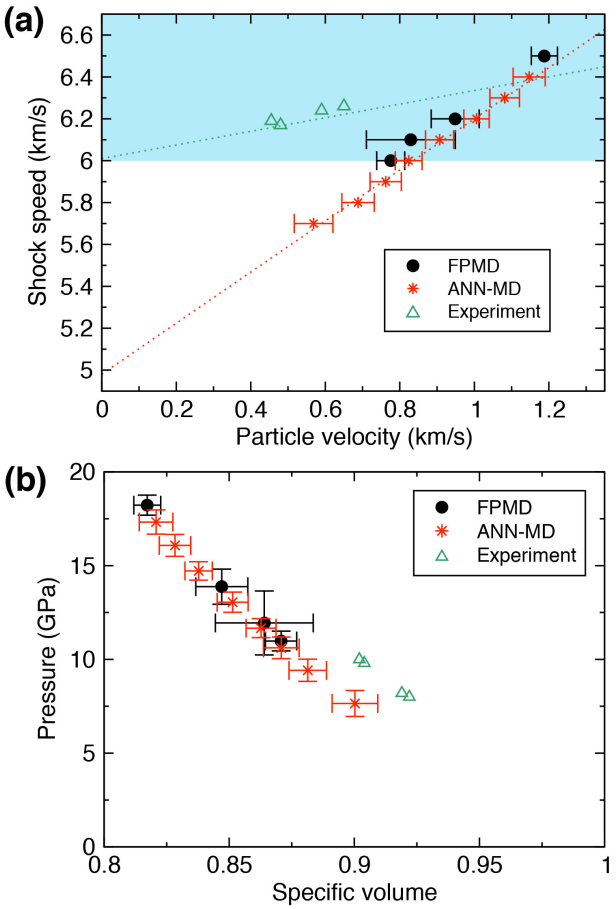

Figure 3. (a) Particle velocity vs. shock speed and (b) pressure vs. specific volume calculated for the shock-induced simulations. The black circles and red stars show the FPMD and ANN-MD results, respectively. The green triangles in (b) are experimental data shown by Wackerle[31]. The red and green dotted lines in (a) are the least-squares fitting lines for the ANN-MD and experimental data, respectively. The blue highlighted area in (a) indicates the shock speed region where FPMD method exhibits elastic deformation behaviors. The error bars indicate standard deviations.

Then we analyzed correlations of particle velocity with shock speed (Figure 3a) and pressure with specific volume (Figure 3b) obtained from the shock simulations of FPMD and ANN-MD. The values plotted in the figures were calculated by average in 1.21 ps for the FPMD, and 24.2 ps for the ANN-MD and CMD. We can see that the elastic properties obtained from ANN-MD are well agreement with the FPMD result. Here we focus on the shock speed range for FPMD and ANN-MD methods. In the FPMD simulations, elastic deformation behaviors cannot be observed for the shock speed less than 6.0 km/s until reasonable simulation time scales. The blue highlighted area in figure 3a indicates shock speed range that was able to reproduce elastic deformation behaviors by FPMD method. On the other hand, Even though the FPMD data used in the learning process is corresponds to the shock speed of above 6.0 km/s, the ANN-MD provided reasonable result for lower shock speed region (outside of the blue highlighted area). The maximum shock speed in the elastic region is little different between the FPMD and ANN-MD results, but the particle velocities are in good agreement with each other. However, as shown with green triangles, the calculation data exhibits a different trend from experimental data for y-cut quartz[31]. Based on the least-squares fitting lines for the ANN-MD and experimental data (dotted lines), difference of the expected elastic wave velocity at an ambient pressure is about 1 km/s. Namely, the model error of the FPMD+MSST method to describe the relation of particle velocity and shock speed is larger than the statistical error. This model error may be ascribed to the approximate exchange-correlation functional. On the other hand, the experimentally measured pressure-volume relations above the specific volume of 0.8 along the shock compression of *y*-cut quartz[31] are also plotted as green triangles in Figure 3b. We can see that our simulations well represents the experimental pressure-volume correlations. However, the highest pressures in first elastic wave region obtained in our simulation are higher than the experimental result. It is considered that surface effects or structural defects existing in the experimental conditions caused this difference. To demonstrate the effects of functional on the shock compression properties, the particles velocity vs. shock speed and pressure vs. specific volume obtained from CMD simulations and FPMD simulations using an exchange-correlation energy

functional based on the local density approximation (LDA) are shown in Figure S2 in the Supporting Information.

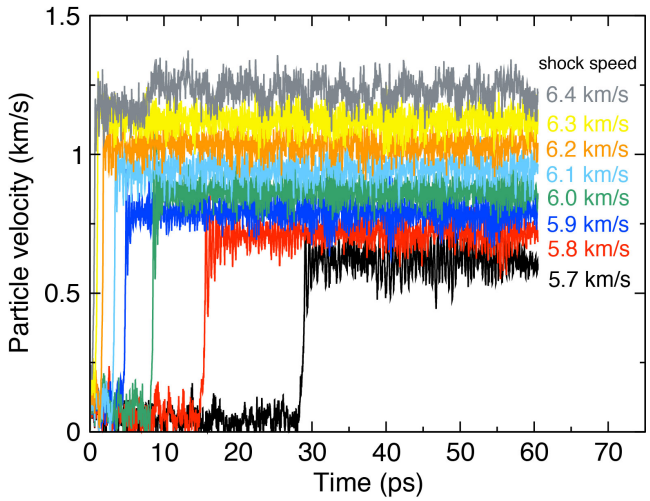

Figure 4. Time evolution of the (a) particle velocity obtained from ANN-MD. The black, red, blue, green, cyan, orange, yellow and gray colors indicate results with the shock speed of 5.7, 5.8, 5.9, 6.0, 6.1, 6.2, 6.3 and 6.4 km/s, respectively.

Finally, Figure 4 shows the time evolution of the particle velocity calculated by ANN-MD shock simulations during 60.5 ps. For the shock speed range from 5.7 to 6.4 km/s, we observed elastic deformation behaviors of α-quartz. Using FPMD method, shock propagation behaviors were not able to observed directory for the shock speed lower than 6.1 km/s during the reasonable computational time. On the other hand, in the ANN-MD, elastic deformation for shock speed of less than 6.1 km/s was observed by long-term simulation for several tens ps. Such delayed convergence of particle velocity is inherent in MSST, and has thus far precluded the application of FPMD+MSST to low-speed shock. This simulation result clearly demonstrates that ANN-potential enabled to represent shock-induced structural deformation reactions under low-shock speed conditions. The same trend is also observed for not only the time evolution of the particles velocity but also that of the uniaxial pressure and specific volume (Figure S3 in the Supporting Information). The convergence values of those quantities are clearly proportional to the shock speed as shown in Figure 3a, looks like that reasonable behavior was produced. To

summarize the shock simulation result, it is shown that the ANN-potential is able to represent the elastic shock wave simulations for a long term with first-principles accuracy.

In this work, we have constructed an ANN-potential and have performed shock simulation of ANN-MD for α-quartz. The created ANN-potential provides reasonable results for energetic and structural properties in un-shocked MD simulation, while the computational time is more than 5,000 times shorter than FPMD simulation. In the shock simulation with this ANN-potential, elastic deformation behaviors of α-quartz were observed with reasonable particle velocity vs. shockspeed and pressure vs. volume correlations. In addition of that, the obtained highest pressure in elastic region is also consistent with FPMD and CMD result. Furthermore, deformation behaviors that take several tens ps are observed in the ANN-MD. FPMD method is not suitable to represent this slow reaction due to its high-computational cost. Those results show that the ANN-potentials are able to apply the research on elastic wave propagation in solid materials, and have a potential application to more complex plastic wave, shear wave and double shock wave propagations. Moreover, our results suggest that ANN-potential can readily be applied to more than two-component systems, because the Chebyshev descriptor that we employed in this work is applicable to multicomponent systems. We are confident that the powerful and efficient ANN-potentials will accelerate research on the elastic properties in complex materials[32-34] and will advance into the research filed of condensed matter physics under extreme conditions in future.

COMPUTATIONAL DETAILS

In this study, all FPMD simulations were carried out using QXMD code[35-36], which is scalable parallel software for FPMD with various extensions including omni-directional MSST[11]. The electronic states in shock-induced α-quartz are calculated using the projector augmented-wave (PAW) method within a framework of DFT[37]. In order to represent exchange-correlation energy, the Perdew-Burke-Ernzerhof (PBE) functional based on generalized gradient approximation (GGA) is employed[38]. As the valence states, 3s, 3p, and 3d states for Si atoms and 2s and 2p

states for O atoms are treated. The plane-wave cutoff energy is 30 and 250 rydberg for wave function and electron density, respectively. The Γ-point only is used for Brillouin zone sampling. Equations of motion are solved via an explicit reversible integrator with a time step of 1.21 fs[39].

To construct ANN-potential for the shock simulation of α-quartz, the ænet package is used for the training process[22]. The potential energies are only used for the potential fitting. The total number of learning data set is about 23,000, including not only shock simulation data but also NPT relaxation processes. Both elastic and plastic deformation structures are included in the shock simulation data. In this work, as the fitting algorithm, the Levenberg-Marquardt method was employed. We used the neural network that consists of 3 hidden layers with 15 nodes for each layer. The "hyperbolic tangent with linear twisting" form given in Ref. 22 is selected as activation functions. The ratio of data for training and testing sets were set to 5:1. We employed the Chebyshev descriptor as the basis function that suggested by Artrith *et al.*[23]. The other detailed parameters are summarized in Table S1 in the Supporting Information. With these conditions, an ANN-potential has been constructed for taking 800 iterations.

This study was supported by JST CREST Grant Number JPMJCR18I2 and JSPS KAKENHI Grant Number 20K14378, Japan. The work at Univ. of Southern California was supported as part of the Computational Materials Sciences Program funded by the U.S. Department of Energy, Office of Science, Basic Energy Sciences, under Award Number DE-SC0014607. The authors thank the Super-computer Center, the Institute for Solid State Physics, University of Tokyo for the use of the facilities. The simulations were also carried out using the facilities of the Research Institute for Information Technology, Kyushu University.

Supporting Information Available: Pair distribution functions including the result of classical molecular dynamics (CMD) simulations, Hugoniot relations including the result of LDA-FPMD and CMD simulations, time evolution of the pressure and specific volume obtained

from the ANN-MD, and parameters for the Levenberg-Marquardt method and basis functions used in the potential training (PDF)

(1) Shen, Y.; Jester, S. B.; Qi, T.; Reed, E. J. Nanosecond Homogeneous Nucleation and Crystal Growth in Shock-Compressed SiO_2. *Nat. Mater.* **2016**, *15*, 60-65.

(2) Kubo, T.; Kato, T.; Higo, Y.; Funakoshi, K. Curious Kinetic Behavior in Silica Polymorphs Solves Seifertite Puzzle in Shocked Meteorite. *Sci. Adv.* **2015**, *1*, No. e1500075.

(3) Panero, W. R.; Benedetti, L. R.; Jeanloz, R. Equation of State of Stishovite and Interpretation of SiO_2 Shock-Compression Data. *J. Geophys. Res.: Solid Earth* **2003**, *108*, No. ECV5.

(4) Mundy, C. J.; Curioni, A.; Goldman, N.; Kuo, I. F. W.; Reed, E. J.; Fried, L. E.; Ianuzzi, M. Ultrafast Transformation of Graphite to Diamond: An Ab Initio Study of Graphite Under Shock Compression. *J. Chem. Phys.* **2008**, *128*, No. 184701.

(5) Gleason, A. E.; Bolme, C. A.; Lee, H. J.; Nagler, B.; Galtier, E.; Milathianaki, D.; Hawreliak, J.; Kraus, R. G.; Eggert, J. H.; Fratanduono, D. E.; *et al.* Ultrafast Visualization of Crystallization and Grain Growth in Shock-Compressed SiO_2. *Nat. Commun.* **2015**, *6*, No. 8191.

(6) Nishiyama, N.; Wakai, F.; Ohfuji, H.; Tamenori, Y.; Murata, H.; Taniguchi, T.; Matsushita, M.; Takahashi, M.; Kulik, E.; Yoshida, K.; *et al.* Fracture-Induced Amorphization of Polycrystalline SiO_2 Stishovite: a Potential Platform for Toughening in Ceramics. *Sci. Rep.* **2014**, *4*, No. 6558.

(7) Yoshida, K.; Wakai, F.; Nishiyama, N.; Sekine, R.; Shinoda, Y.; Akatsu, T.; Nagoshi, T.; Sone, M. Large Increase in Fracture Resistance of Stishovite with Crack Extension Less than One Micrometer. *Sci. Rep.* **2015**, *5*, No. 10993.

(8) Yoshida, K.; Nishiyama, N.; Sone, M.; Wakai, F. Strength and Toughness of Nanocrystalline SiO_2 Stishovite Toughened by Fracture-Induced Amorphization. *Acta Mater.* **2017**, *124*, 316-324.

(9) Misawa, M.; Ryuo, E.; Yoshida, K.; Kalia, R. K.; Nakano, A.; Nishiyama, N.; Shimojo, F.; Vashishta, P.; Wakai, F. Picosecond Amorphization of SiO_2 Stishovite under Tension. *Sci. Adv.* **2017**, *3*, No. e1602339.

(10) Reed, E. J.; Fried, L. E.; Joannopoulos, J. D. A Method for Tractable Dynamical Studies of Single and Double Shock Compression. *Phys. Rev. Lett.* **2003**, *90*, No. 235503.

(11) Shimamura, K.; Misawa, M.; Ohmura, S.; Shimojo, F.; Kalia, R. K.; Nakano, A.; Vashishta, P. Crystalline Anisotropy of Shock-Induced Phenomena: Omni-Directional Multiscale Shock Technique. *Appl. Phys. Lett.* **2016**, *108*, No. 071901.

(12) Shimamura, K.; Misawa, M.; Li, Y.; Kalia, R. K.; Nakano, A.; Shimojo, F.; Vashishta, P. A Crossover in Anisotropic Nanomechanochemistry of Van Der Waals Crystals. *Appl. Phys. Lett.* **2015**, *107*, No. 231903.

(13) Ge, N. N.; Wei, Y. K.; Song, Z. F.; Chen, X. R.; Ji, G. F.; Zhao, F.; Wei, D. Q. Anisotropic Responses and Initial Decomposition of Condensed-Phase β-HMX under Shock Loadings via Molecular Dynamics Simulations in Conjunction with Multiscale Shock Technique. *J. Phys. Chem. B* **2014**, *118*, 8691-8699.

(14) Shimojo, F.; Hattori, S.; Kalia, R. K.; Kunaseth, M.; Mou, W. W.; Nakano, A.; Nomura, K.; Ohmura, S.; Rajak, P.; Shimamura, K.; *et al.* A Divide-Conquer-Recombine Algorithmic Paradigm for Large Spatiotemporal Quantum Molecular Dynamics Simulations. *J. Chem. Phys.* **2014**, *140*, No. 18A529.

(15) Yamada, S.; Shimojo, F.; Akashi, R.; Tsuneyuki, S. Efficient Method for Calculating Spatially Extended Electronic States of Large Systems with a Divide-and-Conquer Approach. *Phys. Rev. B* **2017**, *95*, No. 045106.

(16) Behler, J.; Lorenz, S.; Reuter, K. Representing Molecule-Surface Interactions with Symmetry-Adapted Neural Networks. *J. Chem. Phys.* **2007**, *127*, No. 014705.

(17) Behler, J.; Parrinello, M. Generalized Neural-Network Representation of High-Dimensional Potential-Energy Surfaces. *Phys. Rev. Lett.* **2007**, *98*, No. 146401.

(18) Artrith, N.; Morawietz, T.; Behler, J. High-Dimensional Neural-Network Potentials for Multicomponent Systems: Applications to Zinc Oxide. *Phys. Rev. B: Condens. Matter Mater. Phys.* **2011**, *83*, No. 153101.

(19) Behler, J. Neural Network Potential-Energy Surfaces in Chemistry: A Tool for Large-Scale Simulations. *Phys. Chem. Chem. Phys.* **2011**, *13*, 17930-17955.

(20) Jose, K. V. J.; Artrith, N.; Behler, J. Construction of High-Dimensional Neural Network Potentials Using Environment-Dependent Atom Pairs. *J. Chem. Phys.* **2012**, *136*, No. 194111.

(21) Behler, J. Constructing High-Dimensional Neural Network Potentials: A Tutorial Review. *Int. J. Quantum Chem.* **2015**, *115*, 1032-1050.

(22) Artrith, N.; Urban, A. An Implementation of Artificial Neural-Network Potentials for Atomistic Materials Simulations: Performance for TiO_2. *Comput. Mater. Sci.* **2016**, *114*, 135-150.

(23) Artrith, N.; Urban, A.; Ceder, G. Efficient and Accurate Machine-Learning Interpolation of Atomic Energies in Compositions with Many Species. *Phys. Rev. B* **2017**, *96*, No. 014112.

(24) Behler, J. Atom-Centered Symmetry Functions for Constructing High-Dimensional Neural Network Potentials. *J. Chem. Phys.* **2011**, *134*, No. 074106.

(25) Van Duin, A. C. T.; Dasgupta, S.; Lorant, F.; Goddard Iii, W. A. ReaxFF: A Reactive Force Field for Hydrocarbons. *J. Phys. Chem. A* **2001**, *105*, 9396-9409.

(26) Nielson, K. D.; Van Duin, A. C. T.; Oxgaard, J.; Deng, W. Q.; Goddard Iii, W. A. Development of the ReaxFF Reactive Force Field for Describing Transition Metal Catalyzed Reactions, with Application to the Initial Stages of the Catalytic Formation of Carbon Nanotubes. *J. Phys. Chem. A* **2005**, *109*, 493-499.

(27) Shakouri, K.; Behler, J.; Meyer, J.; Kroes, G. J. Accurate Neural Network Description of Surface Phonons in Reactive Gas-Surface Dynamics: N_2 + Ru(0001). *J. Phys. Chem. Lett.* **2017**, *8*, 2131-2136.

(28) Hellström, M.; Ceriotti, M.; Behler, J. Nuclear Quantum Effects in Sodium Hydroxide Solutions from Neural Network Molecular Dynamics Simulations. *J. Phys. Chem. B* **2018**, *122*, 10158-10171.

(29) Quaranta, V.; Hellström, M.; Behler, J.; Kullgren, J.; Mitev, P. D.; Hermansson, K. Maximally Resolved Anharmonic OH Vibrational Spectrum of the Water/ZnO(10 1 0)

Interface from a High-Dimensional Neural Network Potential. *J. Chem. Phys.* **2018**, *148*, No. 241720.

(30) Shimamura, K.; Fukushima, S.; Koura, A.; Shimojo, F.; Misawa, M.; Kalia, R. K.; Nakano, A.; Vashishta, P.; Matsubara, T.; Tanaka, S. Guidelines for Creating Artificial Neural Network Empirical Interatomic Potential from First-Principles Molecular Dynamics Data Under Specific Conditions and Its Application to α-Ag_2Se. *J. Chem. Phys.* **2019**, *151*, No. 124303.

(31) Wackerle, J. Shock-Wave Compression of Quartz. *J. Appl. Phys.* **1962**, *33*, 922-937.

(32) Inui, M.; Baron, A. Q. R.; Kajihara, Y.; Matsuda, K.; Hosokawa, S.; Kimura, K.; Tsuchiya, Y.; Shimojo, F.; Yao, M.; Tsutsui, S.; *et al.* Viscoelastic Anomaly Accompanying Anti-Crossing Behaviour in Liquid As_2Se_3. *J. Phys.: Condens. Matter* **2018**, *30*, No. 28LT02.

(33) Choudhary, K.; Cheon, G.; Reed, E.; Tavazza, F. Elastic Properties of Bulk and Low-Dimensional Materials Using Van Der Waals Density Functional. *Phys. Rev. B* **2018**, *98*, No. 014107.

(34) Hsu, H.; Umemoto, K.; Wu, Z.; Wentzcovitch, R. M. Spin-State Crossover of Iron in Lower-Mantle Minerals: Results of DFT+U Investigations. *Rev. Mineral. Geochem.* **2010**, *71*, 169-199.

(35) Shimojo, F.; Kalia, R. K.; Nakano, A.; Vashishta, P. Linear-Scaling Density-Functional-Theory Calculations of Electronic Structure Based on Real-Space Grids: Design, Analysis, and Scalability Test of Parallel Algorithms. *Comput. Phys. Commun.* **2001**, *140*, 303-314.

(36) Shimojo, F.; Fukushima, S.; Kumazoe, H.; Misawa, M.; Ohmura, S.; Rajak, P.; Shimamura, K.; Bassman, L.; Tiwari, S.; Kalia, R. K.; *et al.* QXMD: An Open-Source Program for Nonadiabatic Quantum Molecular Dynamics. *SoftwareX* **2019**, *10*, No. 100307.

(37) Blöchl, P. E. Projector Augmented-Wave Method. *Phys. Rev. B* **1994**, *50*, 17953-17979.

(38) Perdew, J. P.; Burke, K.; Ernzerhof, M. Generalized Gradient Approximation Made Simple. *Phys. Rev. Lett.* **1996**, *77*, 3865-3868.

(39) Martyna, G. J.; Klein, M. L.; Tuckerman, M. Nose-Hoover Chains - the Canonical Ensemble via Continuous Dynamics. *J. Chem. Phys.* **1992**, *97*, 2635-2643.